Earth and Planetary Science Letters 495 (2018) 69–78

Contents lists available at ScienceDirect

Earth and Planetary Science Letters

www.elsevier.com/locate/epsl

Local insolation changes enhance Antarctic interglacials: Insights from an 800,000-year ice sheet simulation with transient climate forcing

Michelle Tigchelaar [a,*], Axel Timmermann [b,c,d], David Pollard [e], Tobias Friedrich [d], Malte Heinemann [f]

[a] Department of Atmospheric Sciences, University of Washington, Seattle, WA, USA
[b] Center for Climate Physics, Institute for Basic Science, Busan, South Korea
[c] Pusan National University, Busan, South Korea
[d] International Pacific Research Center, University of Hawai'i at Mānoa, Honolulu, HI, USA
[e] Earth and Environmental Systems Institute, Pennsylvania State University, University Park, PA, USA
[f] Institute of Geosciences, Kiel University, Kiel, Germany

ARTICLE INFO

Article history:
Received 23 October 2017
Received in revised form 29 April 2018
Accepted 1 May 2018
Available online 16 May 2018
Editor: D. Vance

Keywords:
Antarctica
ice sheet
precession
sea level
Quaternary
glacial cycles

ABSTRACT

The Antarctic ice sheet – storing ~27 million cubic kilometres of ice – has the potential to contribute greatly to future sea level rise; yet its past evolution and sensitivity to long-term climatic drivers remain poorly understood and constrained. In particular, a long-standing debate questions whether Antarctic climate and ice volume respond mostly to changes in global sea level and atmospheric greenhouse gas concentrations or to local insolation changes. So far, long-term Antarctic simulations have used proxy-based parameterizations of climatic drivers, presuming that external forcings are synchronous and spatially uniform. Here for the first time we use a transient, three-dimensional climate simulation over the last eight glacial cycles to drive an Antarctic ice sheet model. We show that the evolution of the Antarctic ice sheet was mostly driven by CO_2 and sea level forcing with a period of about 100,000 yr, synchronizing both hemispheres. However, on precessional time scales, local insolation forcing drives additional mass loss during periods of high sea level and CO_2, enhancing the Antarctic interglacial and putting northern and southern ice sheet variability temporarily out of phase. In our simulations, partial collapses of the West Antarctic ice sheet during warm interglacials are only simulated with unrealistically large Southern Ocean subsurface warming exceeding ~4 °C. Overall, our results further elucidate the complex interplay of global and local forcings in driving Late Quaternary Antarctic ice sheet evolution, and the unique and overlooked role of precession therein.

1. Introduction

Understanding the sensitivity of the Antarctic ice sheet (AIS) – which stores enough water to raise global sea level by tens of meters – to climate change is critical; yet its past evolution and the drivers thereof remain poorly constrained. During the Late Quaternary (roughly the past one million years), global climate alternated between cold glacials and warm interglacials with a period of approximately 100,000 yr (100 ka) and corresponding global sea level changes of more than 120 m (Waelbroeck et al., 2002) (Fig. 1a). Most of these changes in sea level are thought to have originated from the Northern Hemisphere (NH) ice sheets. Still, the Antarctic contribution to glacial sea level drops is estimated to be more than 10 m, with the glacial Antarctic grounding line extending up to the continental shelf break (Bentley et al., 2014). During some previous interglacials the polar ice sheets were smaller than presently by 6–9 m sea level equivalent (SLE) ice volume (Dutton et al., 2015). A portion of these past sea level highstands has been attributed to Antarctic ice sheet variability (Dutton et al., 2015; Golledge et al., 2014; Mercer, 1981) – supported by geological evidence suggesting that the West Antarctic ice sheet (WAIS) collapsed (partially) multiple times during the Quaternary (McKay et al., 2012) – but the climatic drivers of this Antarctic ice loss have not yet been identified.

Glacial–interglacial climate variability ultimately derives from periodic changes in insolation caused by variations in the earth's orbit and tilt (Laskar et al., 2004; Milankovitch, 1941). Precession drives seasonal insolation changes with a period of ~21 ka that are modulated by eccentricity, and anti-phased between the hemispheres (Fig. 1a). Annual mean insolation changes are mostly

* Corresponding author.
E-mail address: tigchelaar@atmos.uw.edu (M. Tigchelaar).

https://doi.org/10.1016/j.epsl.2018.05.004
0012-821X/

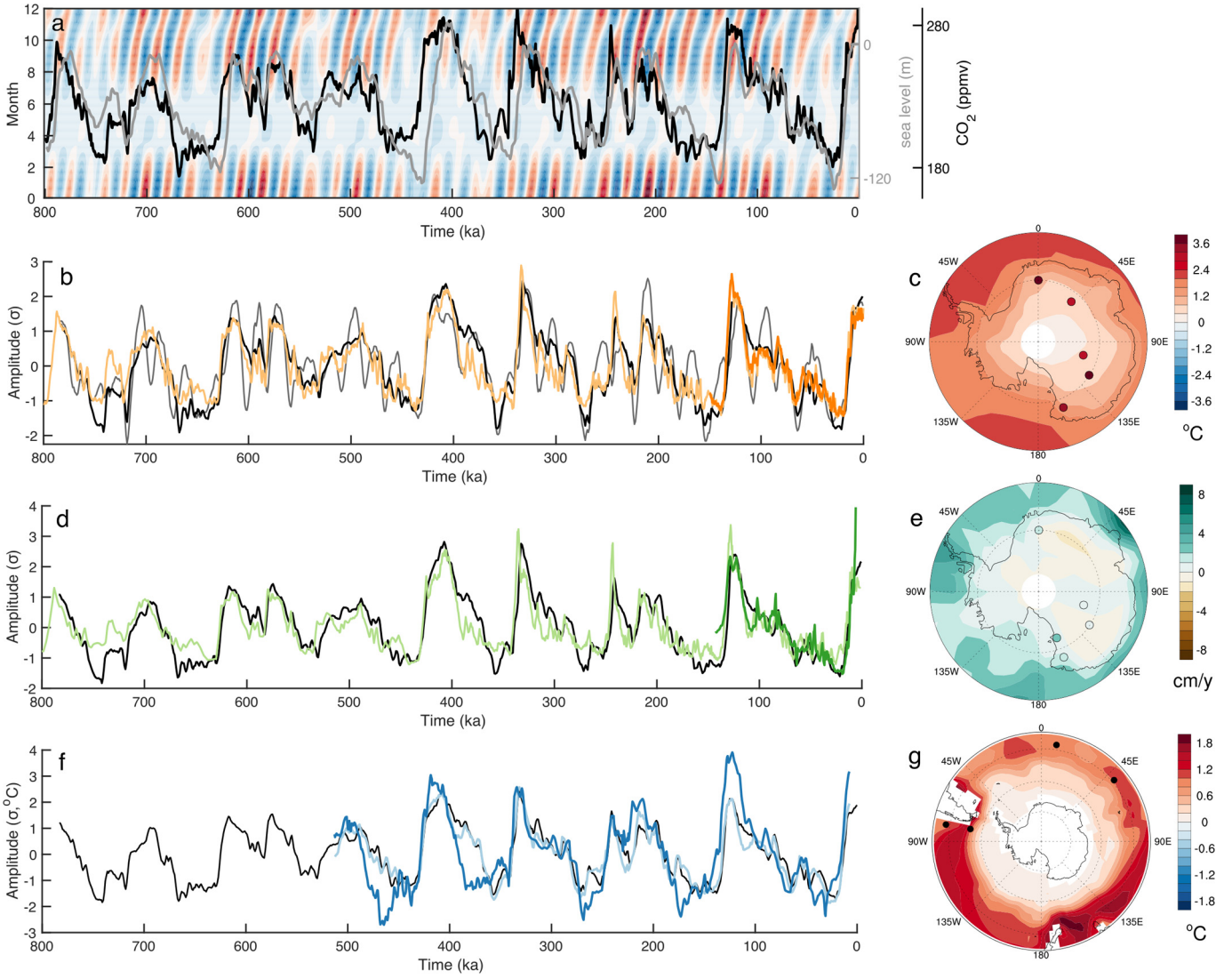

Fig. 1. Southern Hemisphere climate response to Late Quaternary forcing. **a**, Daily insolation anomalies at 65°S resulting from orbital forcing (shading; colours range from −65 to +65 Wm^{-2}) (Laskar et al., 2004), global sea level forcing (grey) (Spratt and Lisiecki, 2016), and CO_2 concentration (black) (Lüthi et al., 2008) over the last 800 ka. **b**, Normalised Principal Component (PC) 1 of modelled annual mean 2 m-air temperatures (black; explained variance (EV) 98.9%), normalised PC1 of modelled annual maximum 2 m-air temperatures (grey; EV 94.5%), normalised PC1 of reconstructed surface air temperatures at five ice core locations (dark orange; 94.0%) (EPICA Community Members, 2006; Jouzel et al., 2007; Kawamura et al., 2007; Parrenin et al., 2004; Stenni et al., 2011; Uemura et al., 2012) and normalised composite of Antarctic surface air temperature reconstructions (light orange) (Parrenin et al., 2013). **c**, EOF1 of modelled annual mean 2 m-air temperatures (shading) and reconstructed surface air temperatures at five ice core locations (dots) (EPICA Community Members, 2006; Jouzel et al., 2007; Kawamura et al., 2007; Parrenin et al., 2004; Stenni et al., 2011; Uemura et al., 2012). **d**, Normalised PC1 of modelled annual mean precipitation (black; EV 83.5%), normalised PC1 of reconstructed accumulation at five ice core locations (dark green; 81.2%) (Bazin et al., 2013; Steig et al., 2000; Vallelonga et al., 2013) and normalised composite of Antarctic accumulation reconstructions (light green) (Bazin et al., 2013; Steig et al., 2000; Vallelonga et al., 2013). **e**, EOF1 of modelled annual mean precipitation (shading) and reconstructed accumulation at five ice core locations (dots) (Bazin et al., 2013; Steig et al., 2000; Vallelonga et al., 2013). **f**, Normalised PC1 of modelled ocean temperatures at 400-m depth (black; 94.6%), composite of modelled SST anomalies (light blue) and composite of reconstructed SST anomalies (dark blue) at four locations (Cortese et al., 2007; Ho et al., 2012; Martínez-Garcia et al., 2009; Nürnberg and Groeneveld, 2006). **g**, EOF1 of modelled ocean temperatures at 400-m depth (shading) and locations of SST reconstructions in f (black dots). Normalised PC1s are in units of standard deviation σ. (For interpretation of the colours in the figure(s), the reader is referred to the web version of this article.)

driven by obliquity forcing at the 41-ka period. Teasing out the causes of AIS variability is complicated by the fact that other components of the earth system also respond to orbital forcing and become additional drivers of Antarctic ice volume changes. For instance, NH ice sheets are thought to be most directly sensitive to changes in NH summer insolation at the precessional period (21 ka) (Milankovitch, 1941), but feedbacks internal to the earth system amplify this insolation forcing and nonlinearly combine into a global climate and carbon cycle response with a period of ∼80–120 ka (Shackleton, 2000). The resulting glacial reduction of atmospheric greenhouse gas concentrations, in particular of CO_2 (Fig. 1a), is an important driver of glacial global cooling, and thus climate variability in Antarctica (Timmermann et al., 2014). At the same time, global sea level variations deriving from NH ice sheet changes also affect the AIS by forcing movement of the grounding line at the 100-ka period (Huybrechts, 2002; Schoof, 2007), while meltwater fluxes associated with northern ice sheet retreat lead to surface warming in the Southern Hemisphere (SH) (He et al., 2013). The relative role of these ice sheet drivers (local insolation changes; remote forcing through changes in global sea level, greenhouse gas concentrations, and NH ice sheets) in driving AIS variability warrants further elucidation and will be the focus of this paper.

Of particular interest here is the role that precession plays in Antarctic climate and ice sheet variability. Raymo et al. (2006) for

example suggest that prior to one million years ago, the AIS was much smaller, with terrestrial margins most sensitive to local summer insolation (Patterson et al., 2014; Pollard and DeConto, 2009); in more recent times, the AIS with its large, buttressing floating ice shelves, would be most vulnerable to changes along its marine margins, including global sea level change (Huybrechts, 2002; Schoof, 2007). Furthermore, scientists have long puzzled over the fact that Antarctic temperature reconstructions contain a precessional component in phase with NH summer insolation (Kawamura et al., 2007). Proposed explanations include a north-south climate connection (He et al., 2013; Kawamura et al., 2007), seasonal rectification by the climate recorder (Laepple et al., 2011), or sensitivity of Antarctic climate to either SH spring insolation (Timmermann et al., 2009) or SH summer length (Huybers, 2009), which have the same phase relationship (Huybers, 2009). These long reconstructions of Antarctic temperatures mostly derive from ice cores in the interior of the East Antarctic ice sheet (EAIS), and limited information is available about long-term climate evolution along Antarctica's marine margins, where the key driving process of Antarctic ice volume are likely to be found.

So far, numerical simulations of AIS evolution have not been set up to adequately evaluate the interplay between these different forcings. Due to the high computational costs of long climate simulations, most modelling studies of past AIS evolution have either used strongly parameterised climate forcings (de Boer et al., 2013; Huybrechts, 2002; Pollard and DeConto, 2009; Ritz et al., 2001); have focused on short time slices, such as part of the Last Interglacial or Last Glacial Maximum (LGM) (DeConto and Pollard, 2016; Golledge et al., 2014); or have applied indexed interpolation between extreme climate states (Maris et al., 2014; Sutter et al., 2016). As a result, these studies mostly ignore the spatial and temporal heterogeneity of Quaternary climate variability or are not set up to simulate the lagged ice sheet response to a transiently evolving climate. A recently completed global climate model simulation of the past 784 ka using the global 3-dimensional earth system model LOVECLIM (Timmermann and Friedrich, 2016) now allows us to simulate for the first time the response of the AIS to fully transient 3-dimensional climate forcing through the various glacial and interglacial climates of the Late Quaternary. Our ice-sheet simulation reveals that Antarctic ice volume mostly responds to global CO_2 and sea level forcing, synchronizing northern and southern ice sheets at the 100-ka period. However, at the precessional period, local summer insolation maxima drive additional mass loss over the Antarctic ice shelves, enhancing interglacials and temporarily desynchronizing northern and southern hemisphere ice-sheet variations.

2. Methods

2.1. Ice sheet model description

Our ice-sheet simulations are done using the Penn State University ice-sheet model (PSU-ISM), a model that has been used extensively for long-term simulations of past and future evolution of the Antarctic ice sheet (DeConto and Pollard, 2016; Pollard and DeConto, 2012). This model uses a hybrid combination of the scaled shallow-ice and shallow-shelf approximations, and calculates the position of the grounding line using an ice flux parameterisation (Schoof, 2007). The model includes vertical diffusion of heat and storage in bedrock below the ice, which is heated from below by a uniform geothermal heat flux for the EAIS and WAIS (Pollard and DeConto, 2012). Basal sliding coefficients are determined by an inverse method, iteratively matching ice-surface elevations to observations until a quasi-equilibrium is reached. Our main simulation is performed on a polar stereographic grid at 20-km resolution.

For present-day simulations, PSU-ISM uses observed annual mean climatologies for atmospheric temperature (1982–2004), accumulation (∼1950–1990) and ocean temperature (1955–2006), with a parameterized sinusoidal seasonal cycle for the atmospheric variables (Pollard and DeConto, 2012). Melting at the ice-ocean interface is parameterized using a direct dependence on ocean temperatures at 400-m depth. For melting at the ice surface, a Positive Degree Day (PDD) scheme is applied to the seasonal cycle of temperature, with an annual refreezing correction (Pollard and DeConto, 2012). Rain and melt water are assumed to freely drain through vertical sub-grid-scale columns of liquid water and can freeze partially or entirely within the ice interior. The model also includes recently added treatments of hydrofracturing and ice cliff failure, which lead to increased calving rates in areas of high surface melt (DeConto and Pollard, 2016).

The mass balance terms in this study include accumulation (snow+rain), total ablation, surface ablation, percolation to the base, basal refreezing, melting at the ice-ocean interface, melting at vertical ocean faces, calving, and cliff failure annually, averaged over the entire ice sheet area. Calving rates reported in the paper also include the cliff failure component. Maps of ice sheet variables are generated from an output file written every 1000 model years.

2.2. Transient climate model experiments

The climate model simulations of the last eight glacial cycles (784 ka to present) have been performed with LOVECLIM (Goosse et al., 2010), a three-dimensional Earth system model of intermediate complexity that has been used for simulations of both present-day and paleo-climate. LOVECLIM consists of a quasi-geostrophic three-level atmospheric model at T21 spectral resolution (∼5.6° × 5.6°), coupled to an ocean general circulation model with 3° × 3° horizontal resolution and twenty vertical levels. The model includes a thermodynamic-dynamic sea ice model and terrestrial vegetation component. While the climate model run follows closely the methodology of Timmermann et al. (2014), in the current simulation the longwave radiative effect of CO_2 was amplified by a factor of 1.97, based on model-proxy comparisons using 63 globally-distributed SST-reconstructions (Friedrich et al., 2016). The resulting net climate sensitivity amounts to ∼4 °C per CO_2 doubling (Timmermann and Friedrich, 2016) and yields a more realistic glacial/interglacial amplitude in surface temperatures compared to paleo-proxy data, such as the records shown in Fig. 1. The climate model is forced with time-evolving orbital parameters (Laskar et al., 2004), high-fidelity ice core reconstructions of atmospheric greenhouse gas concentrations (CO_2, CH_4 and N_2O) (Lüthi et al., 2008) and time-evolving ice sheets in the Northern Hemisphere (Timmermann et al., 2014), using an acceleration factor of five (Timm and Timmermann, 2007). The acceleration technique is based on the assumption of relatively fast equilibration of surface variables to slow external drivers; it thus mostly affects the representation of deep ocean currents (Timm and Timmermann, 2007), but not of surface and thermocline processes that matter for our experiments. In the LOVECLIM simulation, the Antarctic ice sheet remains set to its present-day size; lapse-rate correction as the ice sheet evolves is done in the ice sheet model.

2.3. Ice sheet simulations with climate forcing

PSU-ISM is initialised by running it into equilibrium with present-day climate conditions (Pollard and DeConto, 2012). After this initialisation, the model is forced with 784 ka of time-evolving sea level derived from a recent Late Pleistocene sea level stack (Spratt and Lisiecki, 2016) along with anomalies of monthly-mean atmospheric temperature and precipitation fields and annual mean

ocean temperatures at 400-m depth. These anomalies are calculated with respect to the climatology over the last 200 LOVECLIM model years (representing 1000 orbital years), projected to the ice sheet model grid. Because the sea level stack uses 5 ka as a tie point for the principal component analysis, values from 5 ka to present are set to 0 m sea level anomaly in the ice sheet model (Fig. 1a).

As in Pollard and DeConto (2012), temperature anomalies are additive, whereas the ratio of past to present-day precipitation is used to avoid negative values:

$$T = T_{exp} + T_{obs} - T_{ctl}$$

$$P = P_{exp} \times P_{obs}/P_{ctl}$$

where T is monthly surface air temperature and P is monthly precipitation. Subscripts 'exp', 'obs' and 'ctl' refer to LOVECLIM experiment, observed modern climatology, and LOVECLIM modern control, respectively. For atmospheric temperatures, a lapse-rate correction of 8.0 °C km^{-1} is applied to correct for differences between LOVECLIM orography and modelled ice-sheet elevation; precipitation is multiplied by a Clausius–Clapeyron factor of $2^{\Delta T/10\,^{\circ}\mathrm{C}}$, with ΔT the temperature lapse-rate correction, to account for the elevation desertification effect (DeConto and Pollard, 2016). The climate fields are updated every 1000 yr, while sea level evolves continuously.

For additional oceanic forcing sensitivity runs, the two-dimensional ocean temperature fields at 400-m depth used to drive the control simulation are replaced with zonal mean SST anomalies at 55°S, where the modelled ocean temperature variability is largest (Fig. 1g). In order to test the thresholds for Marine Ice Sheet Instabilities, these anomalies are then multiplied one, two, five and ten times to generate forcing time series with large temperature amplitude, with the limit that ocean temperatures cannot drop below their local freezing point. Finally, we also conducted a simulation over the last 408 ka which uses the parameterized sea level and climate forcing of Pollard and DeConto (2009) with the current version of the PSU-ISM. The sensitivity runs were done at 40-km resolution.

3. Results

3.1. Antarctic climate variability

We use principal component analysis of climate model output and reconstructions to characterize how the orbital and greenhouse gas changes of the Late Quaternary shape climate in the high southern latitudes. Principal component analysis finds orthogonal projections that maximize the variance, reducing high-dimensional data into the spatiotemporal patterns that explain most of the variability. Both changes in reconstructed annual mean temperature over Antarctica and those simulated by the LOVECLIM earth system model (Methods) closely follow the variability in atmospheric CO_2 (Fig. 1b) (Parrenin et al., 2013; Timmermann et al., 2014). At this dominant ~100-ka periodicity, temperatures change sign homogeneously over the Antarctic continent (Fig. 1c), with a simulated glacial–interglacial amplitude of ~4–8 °C. The modelled amplitude is a factor two lower than temperature reconstructions from ice cores, which also include the lapse rate response to evolving ice sheet height. Modelled changes in annual maximum temperature have a much more pronounced precessional component, in phase with SH summer insolation (Fig. 1b); their amplitude is as large as or larger than the annual mean changes (SI Fig. 1). Precipitation over Antarctica is largely limited by the water-holding capacity of the atmosphere, and as such decreases during cold climates, in pace with annual mean temperature and global climate (Fig. 1d, e) (Bazin et al., 2013).

In addition to atmospheric temperature and precipitation, the ice sheet also responds to changes in ocean temperature and circulation in the cavities below ice shelves (200–1000 m). In our climate model simulation, the glacial reduction in ocean temperature at 400-m depth is in phase with atmospheric temperature changes and has a fairly low amplitude (<0.8 °C) close to Antarctica due to the insulating effect of sea ice cover (Fig. 1f, g). Validation against reconstructions is obstructed by the absence of long ocean temperature records at depth and in the proximity of the Antarctic continent. Comparison of annual mean sea surface temperature (SST) changes in the mid-latitude Southern Ocean shows a reasonable agreement of modelled changes with reconstructed values (Fig. 1f), though this comparison is complicated by the fact that the latter likely contain a strong seasonal bias.

3.2. Antarctic ice sheet response to Late Quaternary climate variability

Combined, the simulated changes in annual mean and seasonal temperature and precipitation, intermediate depth ocean temperatures and reconstructions of global sea level, illustrated in Fig. 1, are used to drive the PSU-ISM over the last eight glacial cycles. The glacial–interglacial amplitude of simulated changes in Antarctic ice volume is ~14 m SLE (Fig. 2a), which is in line with previous model estimates (Huybrechts, 2002; Maris et al., 2014; Pollard and DeConto, 2009). The Antarctic ice sheet clearly evolves with a ~100-ka periodicity, with the largest variability in ice sheet height occurring over the WAIS, especially in the Weddell sector and the western part of the Ross embayment (Fig. 2b). Maximum glacial–interglacial ice thickness differences in these areas reach values of more than 2000 m. In contrast, elevation changes over the interior East Antarctic ice sheet (EAIS) are either small or opposite in sign (Fig. 2b). Huybrechts (2002) also describe negative EAIS elevation changes at the LGM, but over a slightly larger area than in our simulation. Since the Huybrechts (2002) simulation uses parameterized climate forcing and different ice sheet dynamics, it is not possible to conclude whether this differential response is due to differences in forcing amplitude or ice flow fields.

During glacial maxima, the AIS grounding line extends to the continental shelf break almost everywhere (Fig. 2b). The simulated local LGM ice volume maximum occurs from 23–20 ka, with the grounding line position at this time generally in close agreement with reconstructions. The last deglaciation begins in the Bellingshausen sector before 16 ka, followed by the Amundsen sector around 13 ka, and the Weddell, Ross and Amery sectors around 10 ka and beyond (SI Fig. 2), a pattern in general agreement with time slice reconstructions of grounding line position (Bentley et al., 2014). However, our retreat in the Ross sector occurs at least ~2 kyr earlier, and further work will focus on this discrepancy. In the Ross sector, there is an "overshoot" of Siple Coast grounding lines at ~6 to 4 ka, and a subsequent re-advance to the modern positions by 0 ka. Similar but more localized behaviour occurs in the Weddell sector (SI Fig. 2). This feature was also described in Maris et al. (2014), and is probably due to time-lagged isostatic bedrock rebound and shallowing grounding lines allowing re-advance in the late Holocene (Bradley et al., 2015).

The minimum extent of the simulated grounding line over the eight glacial cycles is found at 210 ka (Fig. 2a) and is very similar to its present-day position (Fig. 2b). Simulated Antarctic ice volume decreases by only 1–2 m SLE (above present) during past warm interglacials, placing it on the lower end of estimates of AIS contributions to interglacial sea level highstands (Dutton et al., 2015) (Fig. 2a). The slow ice sheet build-up and rapid retreat, and the diachronous behaviour of the East and West AIS, can be seen more clearly in SI Animation 1. Interestingly, the simulated Antarctic ice volume shows substantial variability on precessional time scales, on top of the ~100-ka period. This ~20 ka variability is in

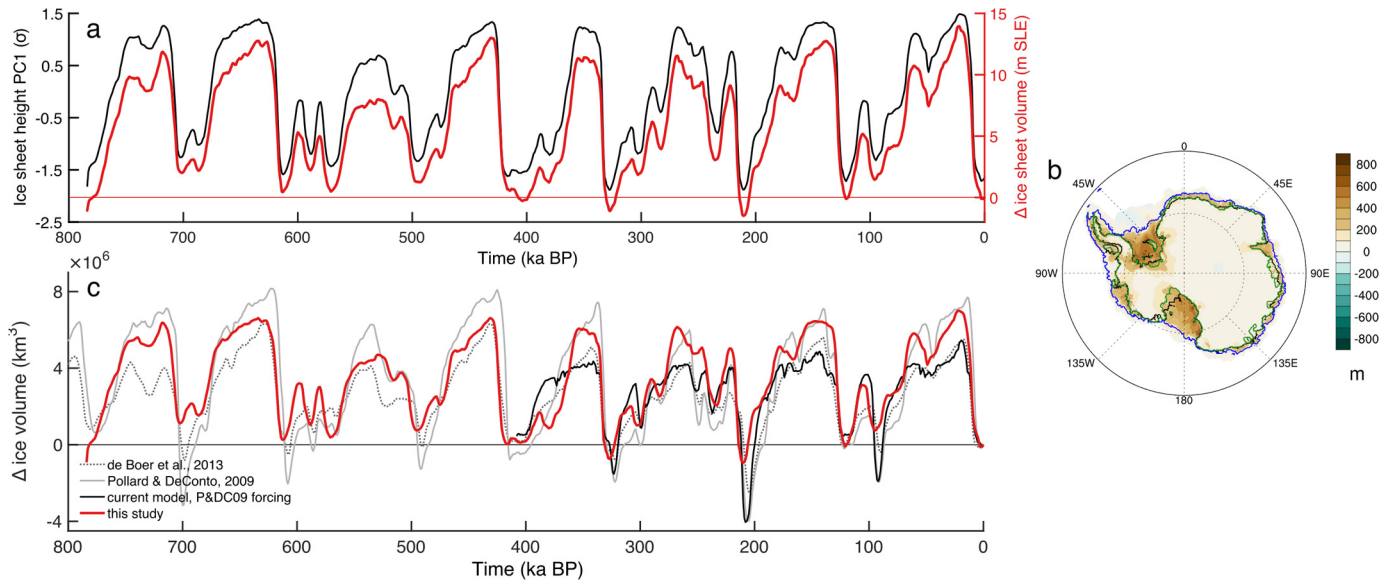

Fig. 2. Antarctic ice sheet response to Late Quaternary forcing. **a**, Normalised PC1 of ice sheet height (black; EV 79.0%) and changes in ice sheet volume in m SLE (red). **b**, EOF1 of modelled ice sheet height (shading), present-day (black), minimum (green; 211 ka) and maximum (blue; 23 ka) grounding line extent. **c**, Modelled changes in ice sheet volume in km^3 in de Boer et al. (2013) (dark grey, dashed); Pollard and DeConto (2009) (light grey, solid); this study (red, solid); and a simulation with this study's version of the PSU-ISM and parameterized climate forcing from Pollard and DeConto (2009) (black, solid). Normalised PC1s are in units of standard deviation σ.

phase with Southern Hemisphere summer insolation (Fig. 1a), as evidenced for example by the strong reduction in ice volume at 95 ka.

Our simulation replaces typically-used parameterized climate forcing with output derived from a transient, three-dimensional climate simulation. Fig. 2c compares our simulation against long-term ice-sheet simulations from Pollard and DeConto (2009), de Boer et al. (2013), and the current PSU-ISM version with Pollard and DeConto (2009) forcing (Methods). Generally, the simulations with parameterized climate forcing simulate lower ice sheet minima. In the case of Pollard and DeConto (2009) this can be attributed to higher amplitudes in parameterized ocean temperature forcing, and an explicit dependence on SH summer insolation, which drives the large reduction in ice volume at e.g., 95 ka. In Pollard and DeConto (2009), the Ross, Weddell, and Amundsen Sea sectors of the WAIS usually advance and retreat in unison, a feature that persists in the run with the current version of the PSU-ISM that uses parameterized climate forcing. This is in contrast to our main simulation presented here, where retreat in the Ross Sea sector typically happens ahead of Weddell Sea retreat (SI Fig. 2; SI Animation 1). This suggests that the spatially heterogeneous climate forcing drives asynchronous evolution of the AIS, a feature that should be further explored with more detailed data-model comparisons and higher resolution simulations of Antarctic climate evolution.

3.3. Mass balance drivers of AIS evolution

The ice sheet model simulation reveals a delicate interplay between global sea level, CO_2, and insolation forcing (Fig. 3). Mostly global sea level and Antarctic ice volume vary in unison, suggesting a synchronization of the Northern and Southern Hemispheres. Certain glacial cycles, such as Marine Isotope Stage (MIS) 11 (~400 ka), however, notably deviate from this interhemispheric synchronization (Fig. 3b), at periods when the sea level and CO_2 forcing are out of phase (Fig. 1a). As noted previously, glacial buildup is slow (Fig. 2a), but glacial retreat occurs rapidly. Fig. 3a shows that retreat happens only when CO_2-levels are above a threshold of ~240 ppm *and* sea level is on the rise.

Through which processes do the combined sea level and greenhouse gas forcing lead to changes in ice sheet volume? When sea level and global temperatures start to drop, such as during MIS 5d (~109 ka), the AIS begins to grow (Figs. 1b, 2a). Changes in sea level do not directly alter the Antarctic mass balance but convert ice near the grounding line between floating ice shelves and grounded ice sheet, which each operate in different dynamical regimes and respond differently to forcing from above and below. A lowering sea level moves the Antarctic grounding line equatorward, limiting the possibility of melting at the ice-ocean interface, thus stabilizing the ice sheet. Calving in the model is primarily a function of ice shelf divergence (DeConto and Pollard, 2016; Pollard and DeConto, 2012). On long time scales, divergence rates – and thus calving rates – in the floating ice shelves stay roughly the same, but since the total area of the grounded ice sheet increases during glacial times, ice-sheet averaged calving rates gradually drop in cold climates (Fig. 4c, SI Fig. 3, SI Fig. 4, SI Anim. 2). In the much colder glacial climate, surface melt rates are near-zero everywhere, allowing for further ice sheet growth (Fig. 4b, SI Fig. 3, SI Fig. 4, SI Anim. 2).

At the end of a glacial period, deglaciation is triggered by rising global sea levels, which cause a grounding line retreat and precondition the ice sheet for melting by turning grounded ice sheet into floating ice shelf. The sea level rise is combined with a sharp rise in surface ablation rates (Fig. 4b, SI Fig. 4, SI Fig. 5, SI Anim. 2). Sufficiently high CO_2 levels are a necessary condition to raise summer temperatures above freezing on the perimeters of the ice sheet, but the lowest Antarctic ice sheet minima (at 327 ka and 210 ka) all occur during periods of minimum precession and high eccentricity, when austral summer insolation is at a maximum (Fig. 1a, Fig. 3, Fig. 4b, SI Fig. 3). Changes in surface melt rates are thus strongly precessionally paced, as revealed by the corresponding power spectrum (Fig. 4g). Because the seasonal effect of precession is anti-phased between the two hemispheres, not all of the northern deglaciations are mirrored in the Southern Hemisphere and vice versa. In particular, Termination III is more pronounced in global sea level, whereas in Antarctica Termination IIIa corresponds to a local ice sheet minimum (Fig. 2). This sensitivity to local summer insolation forcing under conditions of high

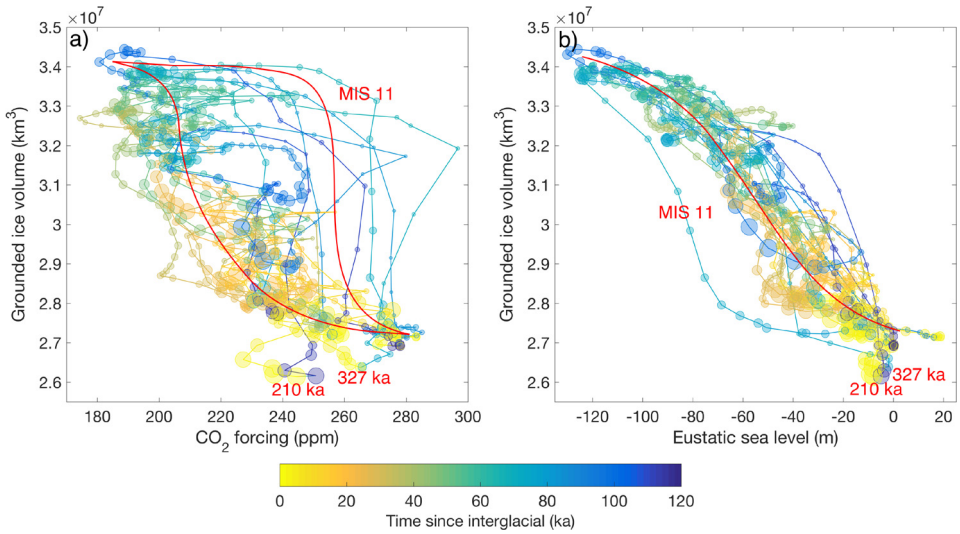

Fig. 3. Antarctic ice volume evolution as a function of external drivers. Antarctic ice volume (km^3) against **a**, CO_2-forcing (ppm) and **b**, global sea level (m). Marker colours indicate time since the last interglacial (ka), while their size indicates the value of the precessional forcing (larger size means stronger austral summer insolation). Red lines are added for emphasis; red labels mark the lowest interglacial ice volumes and hysteresis behaviour during MIS 11 (~400 ka).

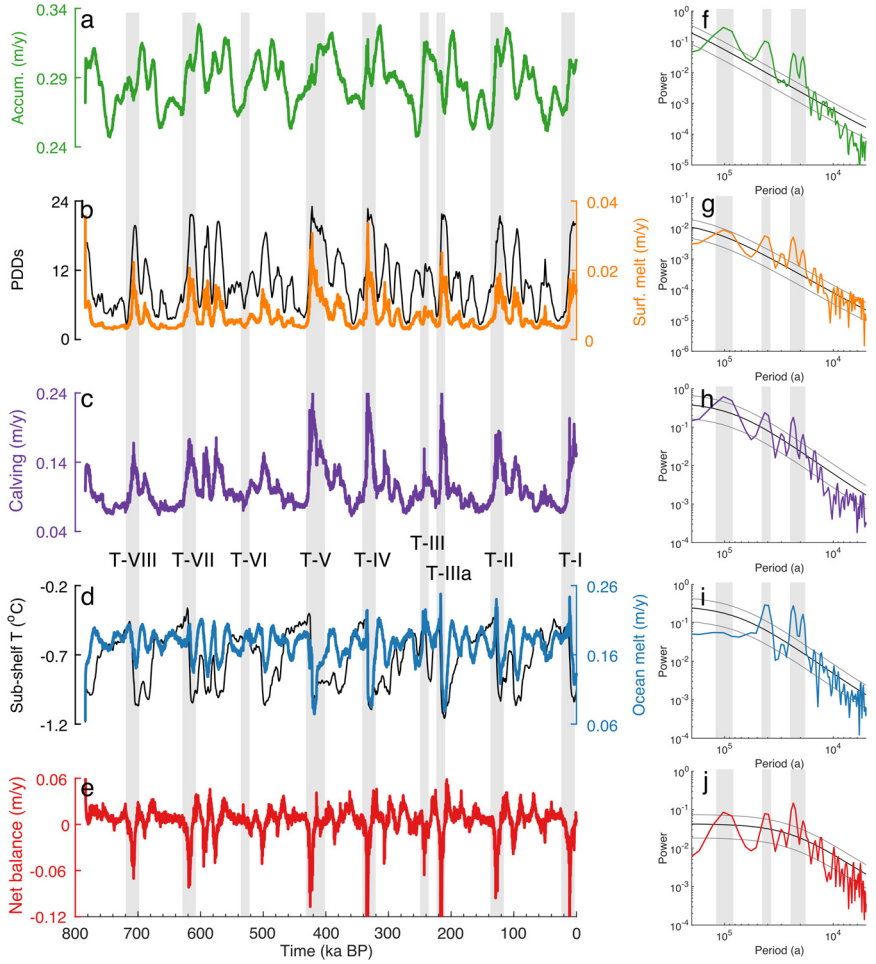

Fig. 4. Evolution of Antarctic average mass balance terms. **a**, Accumulation rate. **b**, Positive Degree Days (PDDs) (black) and surface melt rate. **c**, Calving rate. **d**, Sub-shelf ocean temperature (black) and sub-shelf oceanic melt rate. **e**, Net mass balance. **f**, Power spectrum corresponding to (a). **g**, Power spectrum corresponding to (b). **h**, Power spectrum corresponding to (c). **i**, Power spectrum corresponding to (d). **j**, Power spectrum corresponding to (e). Power spectra are calculated using the Welch Method with a Hanning Window of length 350 ka; black lines represent a red noise power spectrum fit to the original data and grey lines the corresponding 95% confidence range.

sea level and CO_2 leads to a desynchronization of bipolar ice-sheet variations (Fig. 3). It should be noted here that surface mass balance changes are calculated using a commonly-used PDD-scheme (Methods), which does not incorporate insolation changes in energy balance calculations, and as such may not capture the full ablation response to orbital forcing (Bauer and Ganopolski, 2017).

The combined importance of sea level preconditioning and surface warming also highlights the critical role that the floating ice shelves play in mitigating the external forcing. As high surface ablation rates melt away the buttressing ice shelves, calving rates increase dramatically as a result of accelerated ice flow and hydrofracturing (DeConto and Pollard, 2016) (Fig. 4c, SI Fig. 3, SI Fig. 4, SI Fig. 5, SI Anim. 2). Despite these sharp peaks in surface ablation and calving rates, the climate forcing does not trigger a runaway Marine Ice Sheet Instability (Schoof, 2007) during any of the simulated interglacials, leaving most of the WAIS intact (see Discussion).

In contrast to the changes in calving and surface melt rates, the accumulation and oceanic melt rate changes are more a function of ice sheet evolution than climatic forcing; that is, they are passive rather than active contributors to the Antarctic mass balance changes. Glacial precipitation is reduced compared to warmer climates (Fig. 1), but this is countered by the fact that average precipitation rates are generally higher at the northern margins of Antarctica. During deglaciations, ice-sheet averaged accumulation rates initially increase as a result of a warming climate, before slightly decreasing again as a result of shrinking ice-sheet area (Fig. 4a, SI Fig. 5, SI Anim. 2). It should be noted here that our uncoupled modelling framework only considers lapse-rate changes in response to advance and retreat of the AIS. Changes in atmospheric circulation and the resulting changes in precipitation would need to be further investigated in a higher-resolution fully-coupled setup.

Along the same lines, given the low amplitude of glacial–interglacial subsurface ocean temperature change close to the Antarctic continent (Fig. 1g) – a result of the sea ice capping – the ocean temperature underneath the marine ice shelves is much more strongly controlled by the latitudinal position of the grounding line – where further north means warmer – than by the glacial climate forcing (Fig. 4d, SI Fig. 4, SI Fig. 5, SI Anim. 2). Ice-sheet averaged oceanic melt rates are therefore counterintuitively higher during glacial times (Kusahara et al., 2015), and further modulated by the strong precessional surface forcing of ice shelf area and an obliquity component, as shown by the power spectrum (Fig. 4i).

4. Discussion

4.1. Precessional forcing of Antarctic climate and ice sheet variability

The role of precession in driving changes in Antarctic climate and ice sheet volume has been a topic of ongoing debate (He et al., 2013; Huybers, 2009; Kawamura et al., 2007; Laepple et al., 2011; Mercer, 1981; Patterson et al., 2014; Raymo et al., 2006; Timmermann et al., 2009). In our climate and ice sheet simulations, we find strong precessional components in SH climate (Fig. 1), various ice sheet mass balance terms (Fig. 4) including the net mass balance (Fig. 4e, j), and total Antarctic ice volume (Fig. 2). Fig. 5 shows how both modelled and reconstructed annual mean temperatures – when filtered in the precessional band – are in phase with NH summer and SH spring insolation. Presumably, this precessional phasing derives from the relatively weak precessional component present in atmospheric CO_2 concentrations (Fig. 1a), which is a major driver of Antarctic temperatures (Timmermann et al., 2014) and mostly in phase with NH summer insolation (Fig. 5). Whether this precessional component in CO_2 derives from processes involving NH summer insolation or SH spring insolation (e.g., through sea ice and ocean circulation changes (Timmermann et al., 2009)) remains an open question that cannot be answered by this study. Additionally, the sensitivity of northern ice sheets to NH summer insolation adds a precessional component to the global sea level forcing with the same phase relationship.

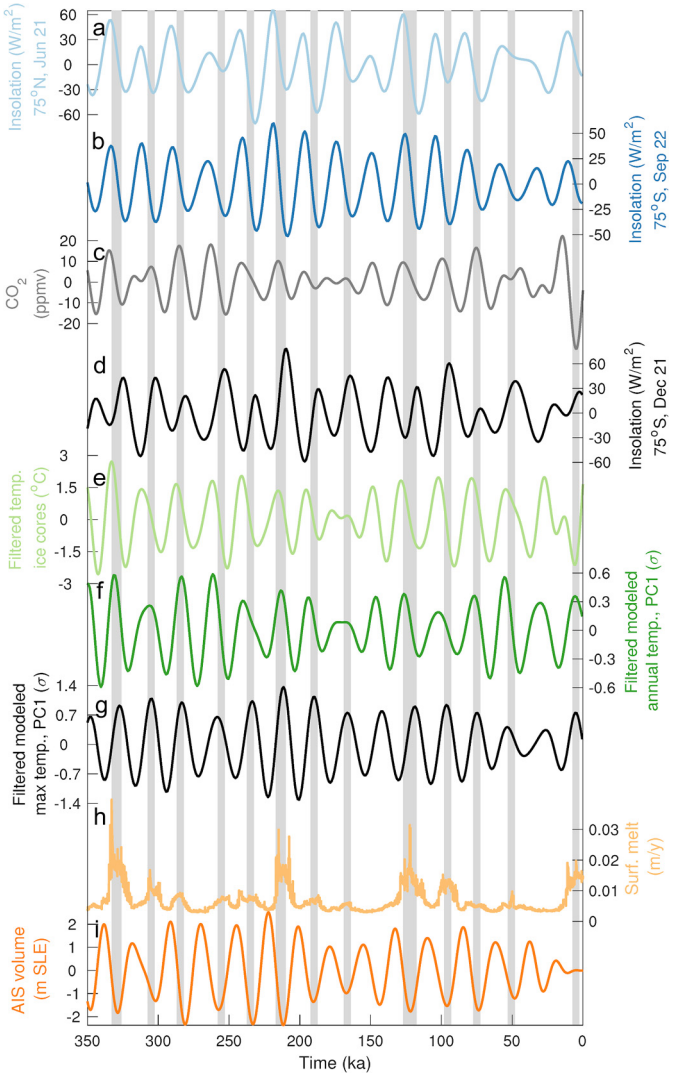

Fig. 5. Precessional phasing of insolation forcing and earth system response. **a**, Insolation (Wm^{-2}) at NH summer solstice (75°N, June 21). **b**, Insolation (Wm^{-2}) at SH spring equinox (75°S, September 22). **c**, CO_2 concentration (Lüthi et al., 2008), filtered in the precessional band. **d**, Insolation (Wm^{-2}) at SH summer solstice (75°S, Dec. 21). **e**, Reconstructed surface air temperatures at five ice core locations (dark orange; 94.0%) (EPICA Community Members, 2006; Jouzel et al., 2007; Kawamura et al., 2007; Parrenin et al., 2004; Stenni et al., 2011; Uemura et al., 2012), filtered in the precessional band. **f**, Normalised PC1 of modelled annual mean 2 m-air temperatures, filtered in the precessional band. **g**, Normalised PC1 of modelled annual maximum 2 m-air temperatures, filtered in the precessional band. **h**, Ice-sheet averaged surface melt rate (my^{-1}). **i**, Antarctic ice volume (m SLE), filtered in the precessional band. Grey bars indicate periods of high surface melt, usually at times of high SH summer temperature and insolation.

Superimposed on this globally synchronized precessional forcing are periods of Antarctic mass loss – including several interglacials with lower-than-present ice volume – that are in phase with SH summer insolation (Figs. 2a, 3, 5). While Antarctic annual mean temperatures are mainly driven by global CO_2, annual maximum temperatures are more closely in phase with local insolation changes (Figs. 1b, 5). It is these seasonal temperature changes that pace the surface melt and calving changes over the Antarctic ice shelves (Figs. 4, 5). Since Antarctic temperatures are generally well below freezing, local insolation forcing can only drive seasonal temperatures high enough to trigger significant surface melt when the background climate is relatively warm (Figs. 1b, 3). As such, summer-insolation driven Antarctic mass loss typically follows periods of rising global CO_2 and sea level and acts to enhance Antarctic ice sheet minima out of phase with the NH ice sheets

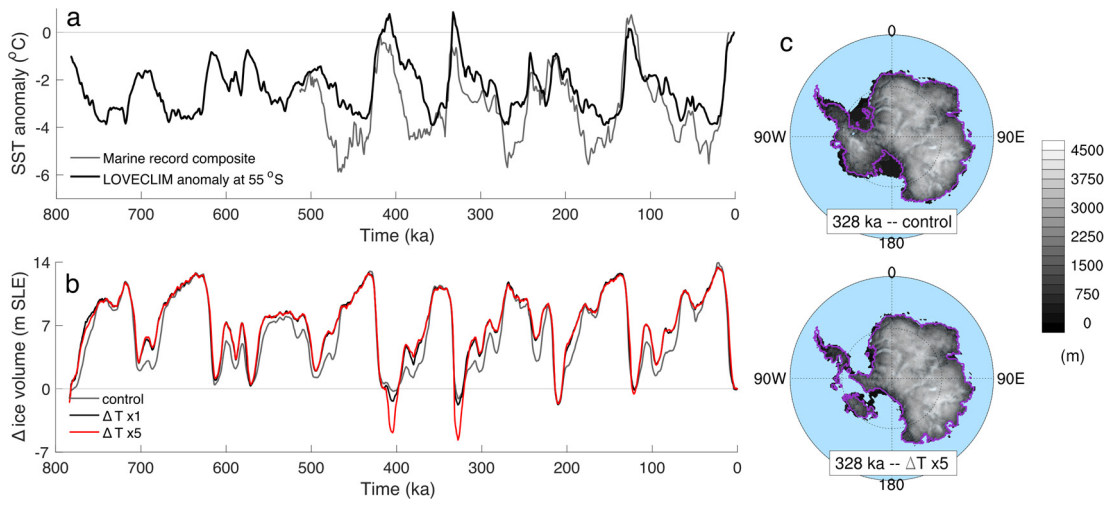

Fig. 6. Ice sheet response to amplified ocean temperature forcing. **a**, Composite of reconstructed SST anomalies (Cortese et al., 2007; Ho et al., 2012; Martínez-Garcia et al., 2009; Nürnberg and Groeneveld, 2006) (grey; Fig. 1g) and modelled zonal mean SST anomalies at 55°S (black). **b**, Changes in Antarctic ice volume in m SLE for the control simulation (grey), a simulation with the temperature forcing from (a) (black), and a simulation with 5× the temperature forcing from (a) (red). **c**, Surface elevation (shading) and grounding line position (purple) at minimum ice volume.

(e.g., Termination IIIa; Figs. 2a, 3). The precessional phasing of the AIS is thus a competition between the precessional component present in global forcing – which is in phase with NH summer and SH spring insolation – and local summer insolation, with the former dominating the overall evolution, but the latter importantly contributing to ice sheet minima (Fig. 5).

4.2. Oceanic contribution to ice sheet evolution

Whereas sea level records suggest that Antarctica may have contributed substantially to past interglacial sea level highstands of >6 m (Dutton et al., 2015), a (partial) collapse of the WAIS does not occur during our climate-model-forced transient ice sheet simulation of the past eight glacial cycles (Fig. 2). This may in part be attributable to the lack of dynamical feedbacks between ice sheet and climate in our offline AIS modelling setup (DeConto and Pollard, 2016), but more importantly it points to a key uncertainty in the oceanic forcing of the ice sheet. Previous modelling studies have been able to simulate interglacial WAIS collapse, but only when applying ad hoc subsurface ocean temperature anomalies reaching levels of 2–5 °C (DeConto and Pollard, 2016; Pollard and DeConto, 2009; Sutter et al., 2016). Reconstructions of mid-latitude Southern Ocean SSTs suggest interglacial warming of several degrees (Capron et al., 2014), but it is not clear to what extent these represent a seasonal signal, or how these anomalies would have travelled to intermediate depth near the Antarctic coastline. Further, recently observed increases in basal melt rates have shown that temperatures on the continental shelf can rise significantly as a result of Circumpolar Deep Water intrusions (Jacobs et al., 2011) – even in the absence of large-scale Southern Ocean warming. One missing piece in our relatively coarse-resolution transient climate model run is the freshwater forcing associated with ice sheet melt: melting of northern ice sheets can lead to Southern Ocean warming through the bipolar seesaw (Stenni et al., 2011), while ice sheet runoff from Antarctica can increase Circumpolar Deep Water intrusion due to sea ice expansion (Golledge et al., 2014).

To determine how much subsurface ocean warming is needed to drive partial collapse of the WAIS, additional sensitivity simulations were conducted. We replaced the two-dimensional ocean temperature forcing with (modelled) zonal mean anomalies from 55°S (Fig. 6a) and multiplied these anomalies by a factor of up to ten to find the threshold for WAIS collapse (Methods). Only at five times amplification of the LOVECLIM simulation subsurface warming, when interglacial ocean temperature anomalies reach values of ∼4 °C, do the oceanic melt rates become sufficiently high to trigger Marine Ice Sheet Instability and subsequent rapid WAIS collapse, leading to a sea level contribution of about 5 m (Fig. 6b, d). This threshold may be lower if ice-atmosphere and ice-ocean feedbacks as well as more regional coastal processes were incorporated in the modelling framework. The ∼4 °C-value is consistent with previous model estimates of Marine Ice Sheet Instability thresholds (DeConto and Pollard, 2016; Sutter et al., 2016). It should be noted that for the amplified forcing, the largest interglacial sea level contributions are simulated at 405 and 328 ka, with limited additional change during the Last Interglacial. Incorporating freshwater forcing in long-term climate simulations, running ice and climate models interactively and with higher resolution, improving model representations of sub-shelf melt processes, and a better understanding of the determinants of near-Antarctic subsurface ocean temperatures will be key steps towards resolving this uncertainty.

5. Conclusion

Until now, long-term (>100 ka) modelling of the AIS has used proxy-based parameterizations for its climatic forcing. Here, for the first time, we have simulated the evolution of the Antarctic ice sheet over the last eight glacial cycles using a transient, three-dimensional climate simulation, meaning that atmospheric, oceanic, and sea level forcing are not by construction synchronous. Our experiment has highlighted the differential roles of, and interactions between, the various external drivers of southern ice sheet variability. Both sea level and CO_2 forcing at the ∼100-ka period are essential drivers of AIS variability, synchronizing the evolution of the Northern Hemisphere ice sheets and Antarctica. On precessional time scales, local summer insolation maxima drive additional mass loss over the Antarctic ice shelves when sea level and annual mean temperature are both high. At these times, and most notably during Terminations IV and III(a), local insolation forcing enhances the Antarctic interglacial, lagging the NH interglacial and putting northern and southern ice sheet variability temporarily out of phase. The Antarctic response to external climate drivers is further modulated by expansion of the ice sheet area against strong mean prevailing latitudinal temperature gradients. The role of ocean temperature forcing in triggering Marine Ice Sheet Insta-

bility and WAIS collapse during past interglacials remains a key uncertainty that will require both better ocean temperature reconstructions and more closely integrated ice sheet-climate modelling frameworks to resolve. Nonetheless, our results uniquely demonstrate the complex interplay of global sea level, atmospheric CO_2, and local insolation forcing in driving Late Quaternary Antarctic ice sheet evolution.

Acknowledgements

This study was supported by National Science Foundation grants #1341311 and 1341394, as well as the Institute for Basic Science (project code IBS-R028-D1). The authors kindly thank Andrey Ganopolski for making available his 800 ka Northern Hemisphere ice sheet simulation results, and Barbara Stenni for sharing the full 314 ka TALDICE oxygen isotope record.

Appendix A. Supplementary material

Supplementary material related to this article can be found online at https://doi.org/10.1016/j.epsl.2018.05.004. The ice sheet model output is available at http://climatedata.ibs.re.kr/data/psu-love/loveanom6-control-784k-20km.

References

Bauer, E., Ganopolski, A., 2017. Comparison of surface mass balance of ice sheets simulated by positive-degree-day method and energy balance approach. Clim. Past 13, 819–832.

Bazin, L., Landais, A., Lemieux-Dudon, B., Toyé Mahamadou Kele, H., Veres, D., Parrenin, F., Martinerie, P., Ritz, C., Capron, E., Lipenkov, V., Loutre, M.F., Raynaud, D., Vinther, B., Svensson, A., Rasmussen, S.O., Severi, M., Blunier, T., Leuenberger, M., Fischer, H., Masson-Delmotte, V., Chappellaz, J., Wolff, E., 2013. An optimized multi-proxy, multi-site Antarctic ice and gas orbital chronology (AICC2012): 120–800 ka. Clim. Past 9, 1715–1731.

Bentley, M.J., Ó Cofaigh, C., Anderson, J.B., Conway, H., Davies, B., Graham, A.G.C., Hillenbrand, C.-D., Hodgson, D.A., Jamieson, S.S.R., Larter, R.D., Mackintosh, A., Smith, J.A., Verleyen, E., Ackert, R.P., Bart, P.J., Berg, S., Brunstein, D., Canals, M., Colhoun, E.A., Crosta, X., Dickens, W.A., Domack, E., Dowdeswell, J.A., Dunbar, R., Ehrmann, W., Evans, J., Favier, V., Fink, D., Fogwill, C.J., Glasser, N.F., Gohl, K., Golledge, N.R., Goodwin, I., Gore, D.B., Greenwood, S.L., Hall, B.L., Hall, K., Hedding, D.W., Hein, A.S., Hocking, E.P., Jakobsson, M., Johnson, J.S., Jomelli, V., Jones, R.S., Klages, J.P., Kristoffersen, Y., Kuhn, G., Leventer, A., Licht, K., Lilly, K., Lindow, J., Livingstone, S.J., Massé, G., McGlone, M.S., McKay, R.M., Melles, M., Miura, H., Mulvaney, R., Nel, W., Nitsche, F.O., O'Brien, P.E., Post Alexandra, L., Roberts, S.J., Saunders, K.M., Selkirk, P.M., Simms, A.R., Spiegel, C., Stolldorf, T.D., Sugden, D.E., van der Putten, N., van Ommen, T., Verfaillie, D., Vyverman, W., Wagner, B., White, D.A., Witus, A.E., Zwartz, D., 2014. A community-based geological reconstruction of Antarctic Ice Sheet deglaciation since the Last Glacial Maximum. Quat. Sci. Rev., 1–9.

Bradley, S.L., Hindmarsh, R.C.A., Whitehouse, P.L., Bentley, M.J., King, M.A., 2015. Low post-glacial rebound rates in the Weddell Sea due to Late Holocene ice-sheet readvance. Earth Planet. Sci. Lett. 413, 79–89.

Capron, E., Govin, A., Stone, E.J., Masson-Delmotte, V., Mulitza, S., Otto-Bliesner, B., Rasmussen, T.L., Sime, L.C., Waelbroeck, C., Wolff, E.W., 2014. Temporal and spatial structure of multi-millennial temperature changes at high latitudes during the Last Interglacial. Quat. Sci. Rev. 103, 116–133.

Cortese, G., Abelmann, A., Gersonde, R., 2007. The last five glacial–interglacial transitions: a high-resolution 450,000-year record from the subantarctic Atlantic. Paleoceanography 22, 1–14.

de Boer, B., van de Wal, R.S.W., Lourens, L.J., Bintanja, R., Reerink, T.J., 2013. A continuous simulation of global ice volume over the past 1 million years with 3-D ice-sheet models. Clim. Dyn. 41, 1365–1384.

DeConto, R.M., Pollard, D., 2016. Contribution of Antarctica to past and future sea-level rise. Nature 531, 591–597.

Dutton, A., Carlson, A.E., Long, A.J., Milne, G.A., Clark, P.U., DeConto, R.M., Horton, B.P., Rahmstorf, S., Raymo, M.E., 2015. Sea-level rise due to polar ice-sheet mass loss during past warm periods. Science 349, 153–162.

EPICA Community Members, 2006. One-to-one coupling of glacial climate variability in Greenland and Antarctica. Nature 444, 195–198.

Friedrich, T., Timmermann, A., Tigchelaar, M., Timm, O.E., Ganopolski, A., 2016. Nonlinear climate sensitivity and its implications for future greenhouse warming. Sci. Adv. 2, e1501923.

Golledge, N.R., Menviel, L., Carter, L., Fogwill, C.J., England, M.H., Cortese, G., Levy, R.H., 2014. Antarctic contribution to meltwater pulse 1A from reduced Southern Ocean overturning. Nat. Commun. 5, 5107.

Goosse, H., Brovkin, V., Fichefet, T., Haarsma, R., Huybrechts, P., Jongma, J.I., Mouchet, A., Selten, F., Barriat, P.-Y., Campin, J.-M., Deleersnijder, E., Driesschaert, E., Goelzer, H., Janssens, I., Loutre, M.-F., Morales Maqueda, M.A., Opsteegh, T., Mathieu, P.-P., Munhoven, G., Pettersson, E.J., Renssen, H., Roche, D.M., Schaeffer, M., Tartinville, B., Timmermann, A., Weber, S.L., 2010. Description of the Earth system Model of Intermediate Complexity LOVECLIM version 1.2. Geosci. Model Dev. 3, 603–633.

He, F., Shakun, J.D., Clark, P.U., Carlson, A.E., Liu, Z., Otto-Bliesner, B.L., Kutzbach, J.E., 2013. Northern Hemisphere forcing of Southern Hemisphere climate during the last deglaciation. Nature 494, 81–85.

Ho, S.L., Mollenhauer, G., Lamy, F., Martínez-Garcia, A., Mohtadi, M., Gersonde, R., Hebbeln, D., Nunez-Ricardo, S., Rosell-Melé, A., Tiedemann, R., 2012. Sea surface temperature variability in the Pacific sector of the Southern Ocean over the past 700 kyr. Paleoceanography 27, 1–15.

Huybers, P., 2009. Antarctica's orbital beat. Science 325, 1085–1086.

Huybrechts, P., 2002. Sea-level changes at the LGM from ice-dynamic reconstructions of the Greenland and Antarctic ice sheets during the glacial cycles. Quat. Sci. Rev. 21, 203–231.

Jacobs, S.S., Jenkins, A., Giulivi, C.F., Dutrieux, P., 2011. Stronger ocean circulation and increased melting under Pine Island Glacier ice shelf. Nat. Geosci. 4, 519–523.

Jouzel, J., Masson-Delmotte, V., Cattani, O., Dreyfus, G., Falourd, S., Hoffmann, G., Minster, B., Nouet, J., Barnola, J.-M., Chappellaz, J., Fischer, H., Gallet, J.C., Johnsen, S.J., Leuenberger, M., Loulergue, L., Luethi, D., Oerter, H., Parrenin, F., Raisbeck, G., Raynaud, D., Schilt, A., Schwander, J., Selmo, E., Souchez, R., Spahni, R., Stauffer, B., Steffensen, J.P., Stenni, B., Stocker, T.F., Tison, J.-L., Werner, M., Wolff, E.W., 2007. Orbital and millennial Antarctic climate variability over the past 800,000 years. Science 317, 793–796.

Kawamura, K., Parrenin, F., Lisiecki, L.E., Uemura, R., Vimeux, F., Severinghaus, J.P., Hutterli, M.A., Nakazawa, T., Aoki, S., Jouzel, J., Raymo, M.E., Matsumoto, K., Nakata, H., Motoyama, H., Fujita, S., Goto-Azuma, K., Fujii, Y., Watanabe, O., 2007. Northern Hemisphere forcing of climatic cycles in Antarctica over the past 360,000 years. Nature 448, 912–916.

Kusahara, K., Sato, T., Oka, A., Obase, T., Greve, R., Abe-Ouchi, A., Hasumi, H., 2015. Modelling the Antarctic marine cryosphere at the Last Glacial Maximum. Ann. Glaciol. 56, 425–435.

Laepple, T., Werner, M., Lohmann, G., 2011. Synchronicity of Antarctic temperatures and local solar insolation on orbital timescales. Nature 471, 91–94.

Laskar, J., Robutel, P., Joutel, F., Gastineau, M., Correia, A.C.M., Levrard, B., 2004. A long-term numerical solution for the insolation quantities of the Earth. Astron. Astrophys. Suppl. Ser. 428, 261–285.

Lüthi, D., Le Floch, M., Bereiter, B., Blunier, T., Barnola, J.-M., Siegenthaler, U., Raynaud, D., Jouzel, J., Fischer, H., Kawamura, K., Stocker, T.F., 2008. High-resolution carbon dioxide concentration record 650,000–800,000 years before present. Nature 453, 379–382.

Maris, M.N.A., de Boer, B., Ligtenberg, S.R.M., Crucifix, M., van de Berg, W.J., Oerlemans, J., 2014. Modelling the evolution of the Antarctic ice sheet since the last interglacial. Cryosphere 8, 1347–1360.

Martínez-Garcia, A., Rosell-Melé, A., Geibert, W., Gersonde, R., Masqué, P., Gaspari, V., Barbante, C., 2009. Links between iron supply, marine productivity, sea surface temperature, and CO_2 over the last 1.1 Ma. Paleoceanography 24, 1–14.

McKay, R.M., Naish, T.R., Powell, R.D., Barrett, P.J., Scherer, R.P., Talarico, F., Kyle, P., Monien, D., Kuhn, G., Jackolski, C., Williams, T., 2012. Pleistocene variability of Antarctic Ice Sheet extent in the Ross Embayment. Quat. Sci. Rev. 34, 93–112.

Mercer, J.H., 1981. West Antarctic ice volume: the interplay of sea level and temperature, and a strandline test for absence of the ice sheet during last interglacial. In: Proceedings of the Canberra Symposium. Sea Level, Ice, and Climatic Change. IAHS, pp. 323–330.

Milankovitch, M., 1941. Kanon der Erdbestrahlung und seine Anwendung auf das Eiszeitenproblem. Royal Serbian Academy Special Publication, vol. 132. Royal Serbian Academy, Belgrade, p. 633.

Nürnberg, D., Groeneveld, J., 2006. Pleistocene variability of the Subtropical Convergence at East Tasman Plateau: evidence from planktonic foraminiferal Mg/Ca (ODP Site 1172A). Geochem. Geophys. Geosyst. 7. https://doi.org/10.1029/2005GC000984.

Parrenin, F., Masson-Delmotte, V., Köhler, P., Raynaud, D., Paillard, D., Schwander, J., Barbante, C., Landais, A., Wegner, A., Jouzel, J., 2013. Synchronous change of atmospheric CO_2 and Antarctic temperature during the last deglacial warming. Science 339, 1060–1063.

Parrenin, F., Rémy, F., Ritz, C., Siegert, M.J., Jouzel, J., 2004. New modeling of the Vostok ice flow line and implication for the glaciological chronology of the Vostok ice core. J. Geophys. Res. D: Atmos. 109. https://doi.org/10.1029/2004JD004561.

Patterson, M.O., McKay, R., Naish, T., Escutia, C., Jimenez-Espejo, F.J., Raymo, M.E., Meyers, S.R., Tauxe, L., Brinkhuis, H., Klaus, A., Fehr, A., Bendle, J.a.P., Bijl, P.K., Bohaty, S.M., Carr, S.a., Dunbar, R.B., Flores, J.a., Gonzalez, J.J., Hayden, T.G., Iwai, M., Katsuki, K., Kong, G.S., Nakai, M., Olney, M.P., Passchier, S., Pekar, S.F., Pross, J., Riesselman, C.R., Röhl, U., Sakai, T., Shrivastava, P.K., Stickley, C.E., Sugasaki, S., Tuo, S., van de Flierdt, T., Welsh, K., Williams, T., Yamane, M., 2014. Orbital forcing of the East Antarctic ice sheet during the Pliocene and Early Pleistocene. Nat. Geosci. 7. https://doi.org/10.1038/ngeo2273.

Pollard, D., DeConto, R.M., 2009. Modelling West Antarctic ice sheet growth and collapse through the past five million years. Nature 458, 329–332.

Pollard, D., DeConto, R.M., 2012. Description of a hybrid ice sheet-shelf model, and application to Antarctica. Geosci. Model Dev. 5, 1273–1295.

Raymo, M.E., Lisiecki, L.E., Nisancioglu, K.H., 2006. Plio-Pleistocene ice volume, Antarctic climate, and the global $\delta^{18}O$ record. Science 313, 492–495.

Ritz, C., Rommelaere, V., Dumas, C., 2001. Modeling the evolution of Antarctic ice sheet over the last 420,000 years: implications for altitude changes in the Vostok region. J. Geophys. Res. 106, 31943–31964.

Schoof, C., 2007. Ice sheet grounding line dynamics: steady states, stability, and hysteresis. J. Geophys. Res., Earth Surf. 112, 1–19.

Shackleton, N.J., 2000. The 100,000-year ice-age cycle identified and found to lag temperature, carbon dioxide and orbital eccentricity. Science 289, 1897–1902.

Spratt, R.M., Lisiecki, L.E., 2016. A Late Pleistocene sea level stack. Clim. Past 12, 1079–1092. https://doi.org/10.5194/cp-12-1079-2016.

Steig, E.J., Morse, D.L., Waddington, E.D., Stuiver, M., Grootes, P.M., Mayewski, P.A., Twickler, M.S., Whitlow, S.I., 2000. Wisconsinan and Holocene climate history from an ice core at Taylor Dome, Western Ross Embayment, Antarctica. Geogr. Ann. 82A, 213–235.

Stenni, B., Buiron, D., Frezzotti, M., Albani, S., Barbante, C., Bard, E., Barnola, J.-M., Baroni, M., Baumgartner, M., Bonazza, M., Capron, E., Castellano, E., Chappellaz, J., Delmonte, B., Falourd, S., Genoni, L., Iacumin, P., Jouzel, J., Kipfstuhl, S., Landais, A., Lemieux-Dudon, B., Maggi, V., Masson-Delmotte, V., Mazzola, C., Minster, B., Montagnat, M., Mulvaney, R., Narcisi, B., Oerter, H., Parrenin, F., Petit, J.-R., Ritz, C., Scarchilli, C., Schilt, A., Schüpbach, S., Schwander, J., Selmo, E., Severi, M., Stocker, T.F., Udisti, R., 2011. Expression of the bipolar see-saw in Antarctic climate records during the last deglaciation. Nat. Geosci. 4, 46–49.

Sutter, J., Gierz, P., Grosfeld, K., Thoma, M., Lohmann, G., 2016. Ocean temperature thresholds for Last Interglacial West Antarctic Ice Sheet collapse. Geophys. Res. Lett. 43, 2016GL067818.

Timm, O.E., Timmermann, A., 2007. Simulation of the last 21,000 years using accelerated transient boundary conditions. J. Climate 20, 4377–4401.

Timmermann, A., Friedrich, T., 2016. Late Pleistocene climate drivers of early human migration. Nature 538, 92–95. https://doi.org/10.1038/nature19365.

Timmermann, A., Friedrich, T., Timm, O.E., Chikamoto, M.O., Abe-Ouchi, A., Ganopolski, A., 2014. Modeling obliquity and CO_2 effects on Southern Hemisphere climate during the past 408 ka. J. Climate 27, 1863–1875.

Timmermann, A., Timm, O.E., Stott, L., Menviel, L., 2009. The roles of CO_2 and orbital forcing in driving Southern Hemispheric temperature variations during the last 21000 yr. J. Climate 22, 1626–1640.

Uemura, R., Masson-Delmotte, V., Jouzel, J., Landais, A., Motoyama, H., Stenni, B., 2012. Ranges of moisture-source temperature estimated from Antarctic ice cores stable isotope records over glacial–interglacial cycles. Clim. Past 8, 1109–1125.

Vallelonga, P., Barbante, C., Cozzi, G., Gabrieli, J., Schüpbach, S., Spolaor, A., Turetta, C., 2013. Iron fluxes to Talos Dome, Antarctica, over the past 200 kyr. Clim. Past 9, 597–604.

Waelbroeck, C., Labeyrie, L., Michel, E., Duplessy, J.C., McManus, J.F., Lambeck, K., Balbon, E., Labracherie, M., 2002. Sea-level and deep water temperature changes derived from benthic foraminifera isotopic records. Quat. Sci. Rev. 21, 295–305.